

# Projection effects in X-ray cores of cooling flow galaxy clusters

Stefano Ettori

Institute of Astronomy, Madingley Road, Cambridge CB3 0HA  
 ESO, Karl-Schwarzschild-Str. 2, D-85748 Garching, Germany  
 settori@eso.org

## ABSTRACT

Recent analyses of *XMM-Newton* and *Chandra* data of the cores of X-ray bright clusters of galaxies show that modeling with a multi-phase gas in which several temperatures and densities are in equilibrium might not be appropriate. Instead, a single-phase model seems able to reproduce properly the spectra collected in annuli from the central region. The measured single-phase temperature profiles indicate a steep positive gradient in the central 100–200 kpc and the gas density shows a flat profile in the central few tens of kpc. Given this observational evidence, we estimate the contribution to the projected-on-the-sky rings from the cluster emissivity as function of the shell volume fraction sampled. We show that the observed projected X-ray emission mimics the multi-phase status of the plasma even though the input distribution is single-phase. This geometrical projection affects (i) analyses of data where insufficient spatial resolution is accessible, (ii) the central bin when its dimension is comparable to the extension of any flatness in the central gas density profile.

**Key words:** galaxies: clustering – X-ray: galaxies.

## 1 INTRODUCTION

The central cooling time of the intracluster X-ray emitting plasma is smaller than the Hubble time for most of the relaxed, nearby systems requiring a flow of cooling gas in the innermost regions to support the overlying gas and maintain the pressure equilibrium (Fabian 1994, Allen et al. 2001). This phenomenon is known as cooling flow and appears in X-ray images as a sharply peaked central surface brightness and in X-ray spectra as lower temperature gas with high intrinsic absorption.

However, a long standing debate is about the real amount of gas deposited in the central region which can be as large as the mass of the central cD galaxy,  $M_{\text{cool}} \approx 10^{12} M_{\odot} (\dot{M}/100 M_{\odot} \text{yr}^{-1})$  (Sarazin 1988, 1997). Correlations are present between the X-ray cooling rate and the strength of star formation in the central galaxy even if the integrated cooling rate up to the radius at which the cooling time becomes more than the Hubble time (i.e. the cooling radius, which is about 100–200  $h_{50}^{-1}$  kpc from the centre) is orders of magnitude larger than the rate of star formation observed only in the inner few tens of kpc (Allen 1995; Mc Namara 1997; Cardiel, Gorgas & Aragon-Salamanca 1998). About 10 per cent of the expected mass deposited in the more massive cooling flow clusters has been now observed in the form of molecular gas warmed to 20–40 K by recently formed stars and located within the inner 50 kpc radius from the cD (Edge 2001).

Recent analyses of the *XMM-Newton* (Jansen et al. 2001) Reflection Grating Spectrometer (RGS) data of the cores of previously well-known cooling flow galaxy clusters like A1795 (Tamura et al. 2001), A1835 (Peterson et al. 2001), Sersic 159-03 (Kaastra et al. 2001), do not show significant emission from gas cooling below 1–2 keV. At the present, it is not clear what stops the gas from cool-

ing further or, conversely, what heats it up. Peterson et al. (2001) and Fabian et al. (2001) discuss possible explanations of the observed drop in the emission from gas at 1–2 keV, which include heating, mixing, differential absorption and inhomogeneous metallicity. Fabian et al. (2001) point out how continuous or sporadic heating creates further problems, such as, e.g., the targeting of the heat at the cooler gas and the high total energy required (but see, e.g., Nulsen et al. 2001 and McNamara et al. 2001).

Moreover, *Chandra* (Weisskopf et al. 2000) Advanced CCD Imaging Spectrometer (ACIS) observation of Hydra-A (David et al. 2001) and analyses of *XMM-Newton* European Photon Imaging Camera (EPIC) spectra of M87, A1835 and A1795 (Molendi & Pizzolato 2001) do not show a wide distribution of gas temperatures in the regions within the cooling radius (except, probably, the central 50 kpc where the cooling time is less than 1 Gyr) as expected from standard multi-phase models. These models assume the intracluster medium is inhomogeneous, with several comoving phases at different temperatures and densities, but in pressure equilibrium, at each radius. Over a typical cooling radius of 200 kpc, the denser, cooler gas cools out of the X-ray band before reaching the cluster centre making the X-ray deposition rate proportional to the radius (see Nulsen 1986 and 1998, Thomas et al. 1987). Furthermore, spectral analyses show strong evidence that the gas can be modeled at the same level of accuracy (or sometimes better; e.g. David et al. 2001, Tamura et al. 2001) with a single-phase instead of a multi-phase emission at each radial annulus (again, this does not apply to the innermost part of the cluster where a multi-phase model appears more appropriate).

Assuming that the single-phase description of the X-ray emitting plasma is more appropriate everywhere in the cluster, and not

arXiv:astro-ph/0111455v1 23 Nov 2001

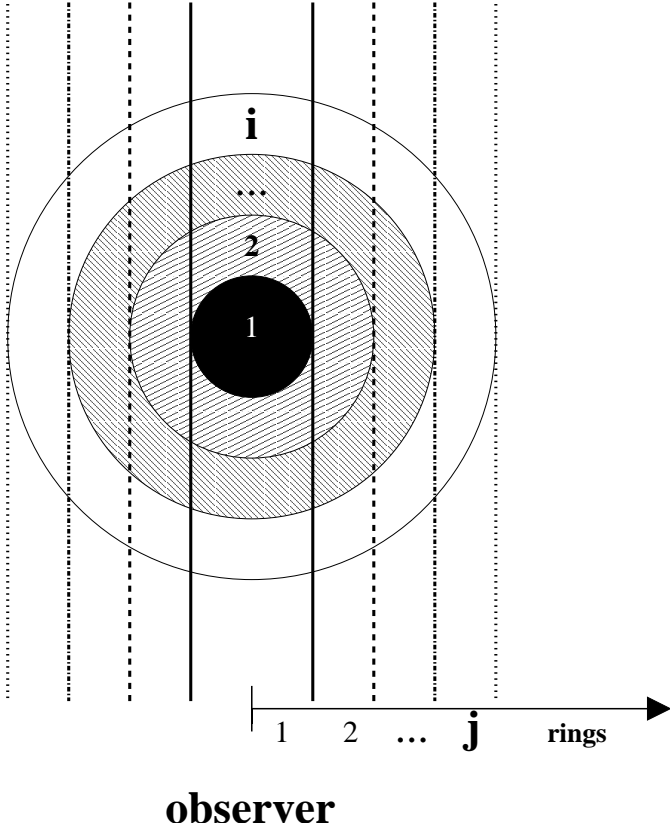


**Figure 1.** Geometrical deprojection. Relation between the shells and the rings.

considering the fate of the gas that is cooling in this way and any other physical phenomenon that is taking place in the cluster core, we have to explain why the multi-phase models have been able to reproduce the observed spectra until now. In this work, we focus on the role played by the geometrical projection on the sky of the cluster core emissivity to mimic a multi-phase gas when the underlying distribution is single-phase. In other words, the purpose of this work is to produce a toy model able to provide an alternative to multi-phase models and check if the assumption of single-phase gas can be ruled out from the results obtained with multi-phase models.

## 2 PROJECTION EFFECTS IN THE OBSERVED SPECTRA

We refer to Kriss, Cioffi & Canizares (1983) and McLaughlin (1999) for details on the calculations of the geometrical deprojection. We define  $V_{ij}$  as the amount of the volume,  $V_i$ , of the shell  $i$  observed through the ring  $j$  adopted in the spectral analysis (cf. Fig. 1).

In each radial ring with area  $A_j$ , a flux  $F_j$  is measured and modeled:

$$F_j = \frac{\sum_{i,\text{shell}} \epsilon_i V_{ij}}{A_j} = \frac{\sum_{i,\text{shell}} n_i^2 \Lambda(T_i) V_{ij}}{A_j}, \quad (1)$$

where  $\epsilon_i$  is the emissivity in shell  $i$ ,  $n_i$  is the gas density and  $\Lambda(T_i)$  is the cooling function. This is proportional to  $T_i^\alpha$ , with  $\alpha$  between  $-0.5$  and  $0.5$  depending on the value of the gas temperature  $T_i$  (the bremsstrahlung continuum with  $\alpha \approx 0.5$  is predominant above 2

keV, whereas the emission from collisionally excited lines mainly contribute to the total emission at lower temperatures).

Therefore, if the gas density profile in the central tens of kpc is flat (or not very steep), then the integrated observed flux can be affected significantly from the shell volume observed. In Fig. 2, the relative volume of the shells seen through each radial ring is normalized to the volume of the inner shell and shows a peak for the inner bins that corresponds to the *second inner shell*.

Hereafter, we use equally spaced bins (or rings). It is worth noting that this is a conservative approach, considering that any progressive increment in the ratio between the outer and the inner ring (e.g. a logarithmic scale), which is an approach generally adopted in data analysis to increase the signal to noise in the fainter outskirts, will imply a larger volume moving outward (cf. Fig. 2).

Given this fact, we can now estimate the differential and total flux measured in each shell and ring, respectively. The null hypothesis that we investigate here is an X-ray emitting plasma represented by a single-phase model, i.e. with a single temperature and density in each shell.

To model physically the intracluster medium, we assume a  $\beta$  model (Cavaliere & Fusco-Femiano 1976) for the density,  $n \propto (1+x^2)^{-1.5\beta}$ , and a power law expression for the temperature:

$$T_i = \begin{cases} T_0(x_i/x_0)^\gamma & x_i < x_t \\ T_0(x_t/x_0)^\gamma = T_t = \text{const} & x_i > x_t \end{cases} \quad (2)$$

It is worth noting that a single  $\beta$  model is not able to represent over a large radial range (e.g. 2 orders of magnitude) the gas density profile obtained from spatial deprojection of the surface brightness of nearby clusters as observed with *Chandra* at high spatial resolution. This is due to the presence in the observed profile of several breaks that mark significant changes in the slope (Allen, Ettori, Fabian 2001, David et al. 2001, Ettori et al. 2001). The  $\beta$  model is however able to properly fit the gas density in the inner region (and where no break is present) over 1 order of magnitude in radius (e.g. from the *Chandra* observation of A1795 presented in Ettori et al. 2001, the gas density profile within 200 kpc is fitted with a  $\beta$ -model with  $\beta = 0.38 \pm 0.01$ ,  $r_c = 33 \pm 2$  kpc and a  $\chi^2$  of 61 with 22 degrees-of-freedom).

We have introduced two scale parameters in units of the core radius,  $r_c$ :  $x_0$  is the spatial resolution element achievable in the spectral analysis and gives the radial width of the central bin,  $x_t$  is the extension of the positive gradient of the gas temperature in the core. From *Chandra* and *XMM-Newton* observations, we note that the spatial resolution element is of the order of 10 kpc for nearby clusters (at redshift 0.05,  $10''$  correspond to  $13 h_{50}^{-1}$  kpc), the core radius is about 30 kpc and the radius at which the temperature reaches a plateau is about 200 kpc, generally consistent with the cooling radius. This implies that  $x_0 \approx 0.3$  and  $x_t \approx 20x_0$ . To investigate the results obtained with previous missions, we study in the next section the case with different values of  $x_0$  and  $x_t$ .

Using the above models in eqn. 1, and renormalizing it with respect to the flux from the inner shell (i.e. no contribution is considered from the outer shells), we can write

$$\frac{F_j}{F_{0j}} = f_j = \sum_{i=\text{shell}} v_i \left(\frac{x_i}{x_0}\right)^{\alpha\gamma} \left(\frac{1+x_0^2}{1+x_i^2}\right)^{3\beta}, \quad (3)$$

where  $v_i$  is the relative volume with respect to the volume of the inner shell as shown in Fig. 2.

Considering equally spaced bins with dimension  $x_0$ , every calculation can be simply performed in the number position of

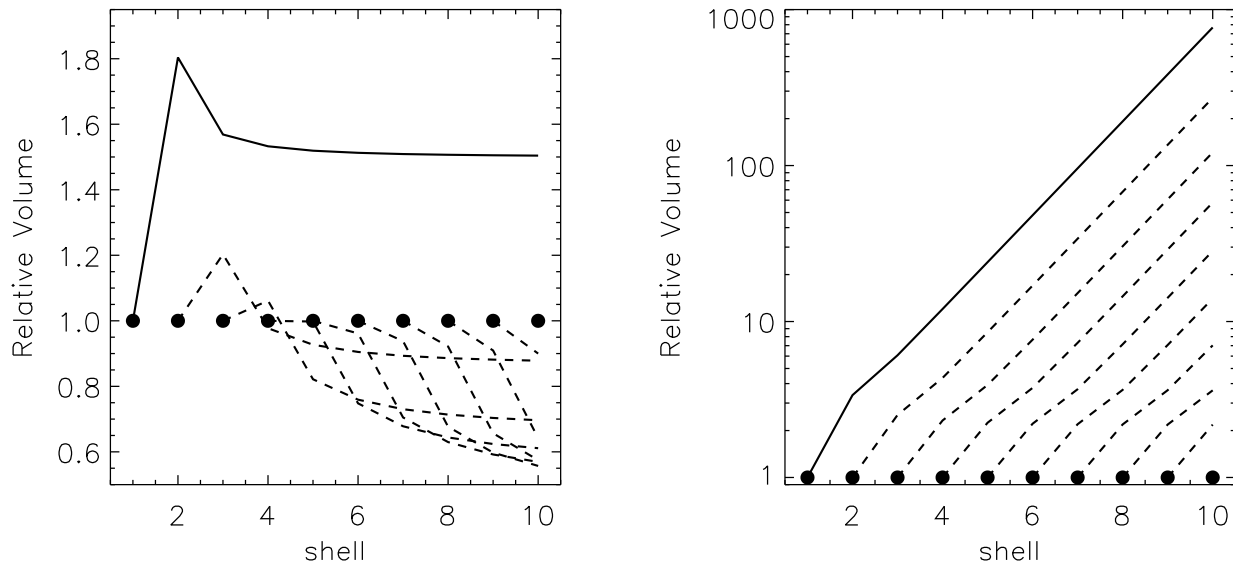


**Figure 2.** Relative volume of the shells, normalized to the volume of the inner shell, seen through each radial ring moving outward from the centre. The solid line represents the inner ring. (Left) Equally spaced bins, (right) doubling the size of the next bin.

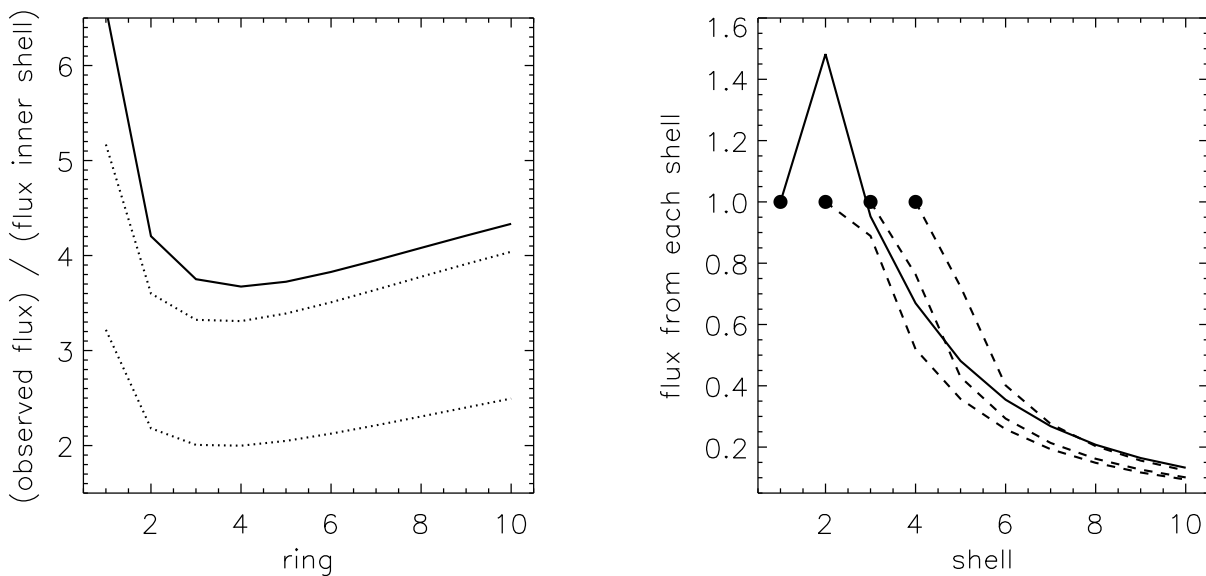


**Figure 3.** (Left) Ratio between the integrated flux observed in each ring and the flux coming from the inner shell seen in that ring. The solid line assumes  $(\alpha, \beta, \gamma) = (0.5, 0.4, 0.2)$ , the two dotted lines  $(-0.5, 0.4, 0.2)$  and  $(0.5, 0.8, 0.2)$  from the top, respectively. (Right) Differential fluxes originating from each shell and normalized to that coming from the inner shell for the first 4 rings. The inner ring (ring 1) is represented by a solid line, the others by dashed lines. For a given ring, the integral of the fluxes along the shells (right panel) is a point in correspondence of that ring in the left panel.

rings/shells. We consider a region of interest extending up to  $1.5 \times x_t$ .

In Fig. 3, we show the estimates of  $f_j$  for  $(\alpha, \beta, \gamma) = (0.5, 0.4, 0.2)$ , typical for plasma in the core regions of nearby clusters observed recently with *Chandra*, e.g. A1795 (Ettori et al. 2001) and Hydra-A (David et al. 2001).

From Fig. 3, it appears that the inner ring exhibits still significant contribution from the outer shells. In particular, shell number

2 has a contribution by a factor of 1.48 relative to shell number 1, whereas numbers 3, 4, ..., 10 (see Fig. 1) have a relative contribution of 0.95, 0.67, ..., 0.13. The outer bins, on the other hand, are dominated by the emission of the central shell with contribution due to exterior shells becoming weaker with increasing radius. For example, the second bin (that collects photons from all the shells apart from the first one and, thus, has the 2nd as innermost shell with respect to which the relative contributions are estimated) has a

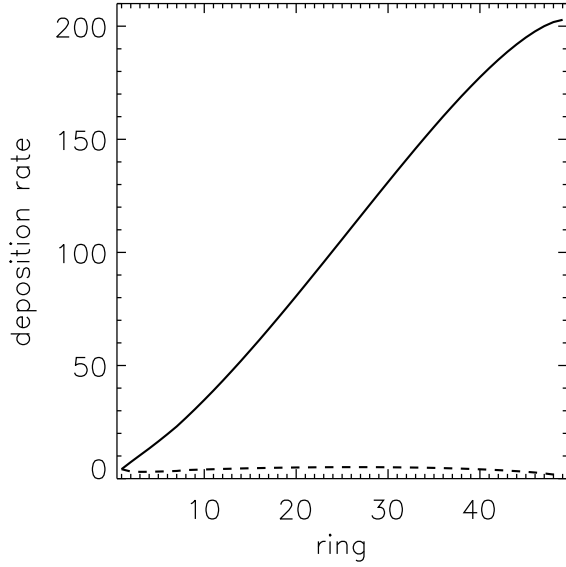


**Figure 4.** Cumulative (solid line) and differential (dashed line) distribution of the mass deposition rate,  $\dot{M}$ , relative to the value in the inner shell.

relative contribution from the 3rd shell of 0.89, while the 3rd, 4th, ..., 10th bins have a relative contribution from the next-to-the-inner shell of about 70 per cent.

The combination of this differential weight in emission with the presence of a positive temperature gradient in the core (cf. eqn. 2) makes necessary the use of a multi-phase (i.e. minimum two-temperatures) model to reproduce the observed flux. A way to parametrize the total emission originating from a multi-phase gas is to use the mass deposition rate,  $\dot{M}$ , that is defined (from Johnstone et al. 1992) as

$$\frac{5}{2} \frac{T_i}{\mu m_p} \dot{M}_{ij} = \epsilon_i V_{ij}, \quad \dot{M}_j = \sum_i \dot{M}_{ij}. \quad (4)$$

The differential and cumulative distribution of  $\dot{M}$  as measured in each ring is plotted in Fig. 4 for  $x_0 = 0.3$  and  $x_t = 10$ . The cumulative distribution increases with radius with a power law index of about 1–1.1 (the dependence on  $x_t$  is minimal). This power law index is fully consistent with both the best-fit observed values of about 1 from spatial deprojection of *ROSAT* PSPC surface brightness profiles combined with *ASCA* spectral analysis (Allen et al. 2001) and values of 0.8 and 1.3 obtained from deposition rate profiles measured with spectral analysis and spatial deprojection, respectively, from *Chandra* data of A1795 (Ettori et al. 2001). It is worth noting that there is a slight dependence of the power law index upon the temperature through the shape of the cooling function which changes from  $-0.5$  to  $0.5$  moving to temperatures higher by a factor that we choose to be 1.5 the central value (this comes from the considerations that (i) observations do not show temperatures lower than 1–2 keV in the core and (ii) bremsstrahlung is predominant at  $T > 2$  keV). This dependence makes the profile flatter in the outskirts, i.e. beyond the radius where we introduce the change in the shape of  $\Lambda(T)$ . (e.g., when  $x_0 = 0.3$  and  $x_t = 10$ , the slope changes from 1.08 to 0.88).

## 2.1 Changing $x_0$ and $x_t$

In this section, we investigate how our results depend on the relative extension of the resolution element,  $x_0$ , and of the temperature gradient,  $x_t$ , with respect to the central flatness in the gas density profile.

Considering the weak dependence of the emissivity upon the temperature, no significant change in the flux distribution is observable upon varying the values of  $x_t$ . However, it is the presence of the temperature gradient that mimics a multi-temperature distribution in the core. The extent of this temperature gradient is proportional to  $x_t/x_0$  (eqn. 2). Therefore, a value of  $x_t$  larger than  $x_0$  is required to resolve it. This is now routinely accessible to present-day missions, like *Chandra* and *Newton-XMM*. In detail, for the well-known behaviour of the angular diameter distance that increases up to redshifts of about 1 and then turns over, the *proper* size of an object resolved with a  $1''$  scale (80 per cent encircled power radius of  $0.7''$  at 1 keV) by *Chandra* and about  $20''$  scale (average of the 80 per cent encircled power radius for energies between 1.5 and 10.5 keV) by *XMM-Newton* is below  $9 h_{50}^{-1}$  kpc and  $\sim 170 h_{50}^{-1}$  kpc, respectively, at any redshift. In Fig. 5, we show the “shell” and projected temperature profiles with the integral emission-weighted temperature up to a given radius. The latter estimate gives an indication of the efficiency in recovering the “shell” temperature when the spatial resolution  $x_0$  is a non-negligible fraction of the extension of the temperature gradient  $x_t$ . Even if the standard cooling flow model is not anymore a complete description of what is happening in the cluster cores, it is worth noticing that the use of this model in spectral analyses for the measurement of the integral emission-weighted temperature within a fixed radius (e.g. Allen & Fabian 1998, Ettori, Allen & Fabian 2001) allows to recover the “shell” temperature at that radius correcting for the presence of the cooler gas.

More noticeable is the influence of  $x_0$ . When  $x_0$  has low values (i.e. the resolution element is smaller than  $r_c$ ), more contribution from outer shells appears as a consequence of the larger volume surveyed (see Fig. 6).

For example, if we enlarge  $r_c$  up to 100 kpc (or reduce the resolution element to 3 kpc) with respect to the original values of 30 (and 10) kpc,  $x_0$  becomes 0.1 and the contribution from shells number 2, 3, ..., 10 relative to shell number 1 in the inner bin are 1.87, 1.60, 1.49, ..., 0.83, respectively. The third bin still has a relative contribution from the 4th shell (with respect to the 3rd one) of a comparable amount (1.01). Starting with the fourth bin, the emission from inner shell (number 4) dominates over the contribution from the next shells (e.g. 5th shell: 0.93, 6th shell: 0.64, ..., 10th shell: 0.35). Consequently, the total observed flux relative to the flux coming from the inner shell increases by a factor between 3.4 and 1.3 and the deposition rate by about 2 in the first 10 rings.

On the contrary,  $x_0 \gtrsim 1$  makes the contribution in emission from the inner shells dominant. When  $x_0 = 1$ , shell 2, 3, ..., 10 contributes 0.64, 0.25, ..., 0.02, respectively, to the 1st ring. All the outer rings have a contribution from the second and third innermost shells of 70 and 40 per cent, respectively. The relative observed flux is about half the one observed for the case  $x_0 = 0.3$ . When  $x_0 > 1$  (this is the case for a given resolution element not able to resolve any flatness in the density profile), then the contribution from the second (third) innermost shell is about 50–70 (20–40) per cent.

Changes in  $x_0$  and  $x_t$  also affect the slope of the mimicked profile of the cumulative deposition rate. For reasonable values of  $x_t$  larger than 5, the larger  $x_0$ , the steeper the profile inside/outside

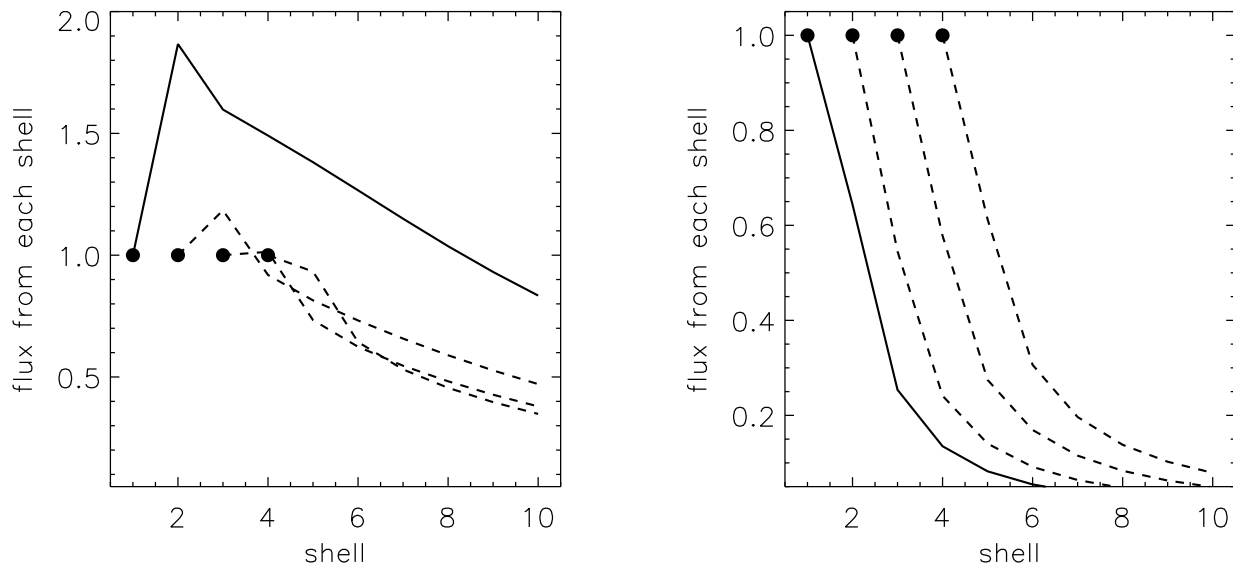


**Figure 6.** Differential fluxes in the first 4 rings as in the right panel in Fig. 3 but with  $x_0 = 0.1$  (left) and 1 (right) instead of 0.3.

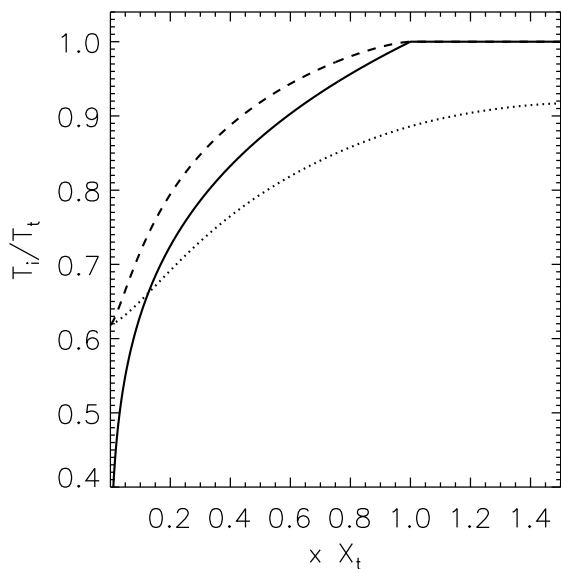


**Figure 5.** “Shell” (solid line) and “projected” (i.e. emission-weighted in each ring; dashed line) temperature profiles. The dotted line indicates the integral emission-weighted temperature measurement, i.e. the estimated temperature value once the “shell” temperature profile is weighted by the differential flux in each shell up to a given radius. For example, at  $0.5 \times x_t$ , the “shell” temperature is  $0.87 \times T_t$ , its projected value at that ring is  $0.92 \times T_t$  and the estimated integrated value for a given detector with resolution  $x_0 = 0.5 \times x_t$  should be  $0.79 \times T_t$ .

the cooling region. For example, the slopes vary from 0.9/0.7 when  $(x_0, x_t) = (0.1, 5)$  to 1.1/1.0 when  $(x_0, x_t) = (1, 10)$ .

### 3 CONCLUSIONS

We have simulated *Chandra* spectra for the inner ring with a combination of MEKAL models (Kaastra 1992, Liedahl et al. 1995) in XSPEC (Arnaud 1996) weighted according to our results in Figs. 3 and 6. We have then fitted both a single MEKAL model and a MEKAL plus intrinsically absorbed cooling flow model. The two models provide a good fit to the data and, at the level of the uncertainties still present, are not distinguishable from a statistical point of view.

We conclude that the combination of a flat gas profile in the central tens of kpc and the volume fraction sampled of the shells in a projected-on-the-sky ring explains the strong evidence of multi-phase intracluster medium whereas the underlying distribution is in a single-phase with a positive temperature gradient in the core. In particular, we show that the central bins are more affected by the geometrical sampling of the volume of the shells and present a large contamination from different gas phases. This could explain the necessity for a cooling flow (multi-phase) component to model the emission from the inner ring of Hydra-A (David et al. 2001) whereas no evidence of multi-phase gas is spectroscopically obtained elsewhere in the cluster. In other words, if there is evidence for a single phase gas in all the rings except the central one, then projection effects play a relevant role in contaminating the central bin contaminated with the overlapping shells. These considerations support the case for a proper deprojection of the cluster emission when the analysis of the central parts is carried out.

### ACKNOWLEDGEMENTS

The author thanks the referee, A. Edge, for giving suggestions in improving the presentation of this work and Glenn Morris for revising the original manuscript.

## REFERENCES

- Allen S.W., 1995, MNRAS, 276, 947
- Allen S.W., Fabian A.C., 1998, MNRAS, 297, L57
- Allen S.W., Fabian A.C., Johnstone R.M., Arnaud K.A., Nulsen P.E.J., 2001, MNRAS, 322, 589
- Allen S.W., Etti S., Fabian A.C., 2001, MNRAS, in press (astro-ph/0008517)
- Arnaud K.A., 1996, "Astronomical Data Analysis Software and Systems V", eds. Jacoby G. and Barnes J., ASP Conf. Series vol. 101, 17
- Cardiel N., Gorgas J., Aragon-Salamanca A., 1998, MNRAS, 298, 977
- Cavaliere A., Fusco-Femiano R., 1976, A&A, 49, 137
- David L.P., Nulsen P.E.J., McNamara B.R., Forman W., Jones C., Ponman T., Robertson B., Wise M., 2001, ApJ, 557, 546
- Edge A.C., 2001, MNRAS, in press (astro-ph/0106225)
- Etti S., Allen S.W., Fabian A.C., 2001, MNRAS, 322, 187
- Etti S., Fabian A.C., Allen S.W., Johnstone R.M., 2001, MNRAS, submitted
- Fabian A.C., 1994, ARAA, 32, 277
- Fabian A.C., Mushotzky R.F., Nulsen P.E.J., Peterson J.R., 2001, MNRAS, 321, L20
- Jansen F. et al., 2001, A&A, 365, L1
- Johnstone R.M., Fabian A.C., Edge A.C., Thomas P.A., 1992, MNRAS, 255, 431
- Kaastra J.S., 1992, *An X-Ray Spectral Code for Optically Thin Plasmas* (Internal SRON-Leiden Report, updated version 2.0)
- Kaastra J.S., Ferrigno C., Tamura T., Paerels F.B.S., Peterson J.R., Mittaz J.P.D., 2001, A&A, 365, L99
- Kriss G.A., Cioffi D.F., Canizares C.R., 1983, ApJ, 272, 439
- Liedahl D.A., Osterheld A.L., Goldstein W.H., 1995, ApJ, 438, L115
- McLaughlin D.E., 1999, AJ, 117, 2398
- Mc Namara B.R., 1997, in "Galactic and Cluster Cooling Flows", ed. N. Soker, San Francisco PASP, 109 (astro-ph/9612196)
- Mc Namara B.R. et al., 2001, ApJ, in press (astro-ph/0110554)
- Molendi S., Pizzolato F., 2001, ApJ, in press (astro-ph/0106552)
- Nulsen P.E.J., 1986, MNRAS, 221, 377
- Nulsen P.E.J., 1998, MNRAS, 297, 1109
- Nulsen P.E.J., David L.P., McNamara B.R., Jones C., Forman W., Wise M., 2001, ApJ, in press (astro-ph/0110523)
- Peterson J.R. et al., 2001, A&A, 365, L104
- Sarazin C.L., 1988, *X-ray emission from clusters of galaxies*, Cambridge University Press
- Sarazin C.L., 1997, in "Workshop on High Throughput X-ray Spectroscopy", ed. P.Sullivan & H. Tanabaum, Smithsonian Astrophysical Observatory (astro-ph/9612049)
- Tamura T. et al., 2001, A&A, 365, L87
- Thomas P.A., Fabian A.C., Nulsen P.E.J., 1987, MNRAS, 228, 973
- Weisskopf M.C., Tanabaum H.D., Van Spebroeck L.P., O' Dell S.L., 2000, Proc SPIE 4012, in press (astro-ph/0004127)